Submitted to Physics Letters B

LBL-2459
Preprint c.2

COMPARISON OF THE REACTIONS $\pi^- p \to p + X$ AND $pp \to p + X$ AT 205 GeV/c

F. C. Winkelmann

December 5, 1973

Prepared for the U. S. Atomic Energy Commission
under Contract W-7405-ENG-48

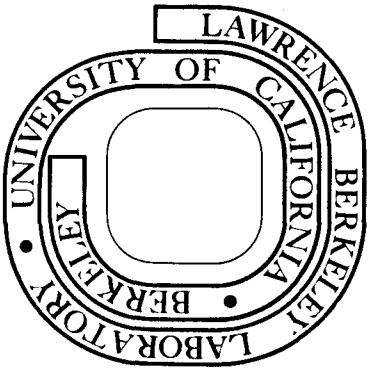

LBL-2459
c.2

DISCLAIMER

LBL-2459

COMPARISON OF THE REACTIONS $\pi^- p \to p + X$ AND $pp \to p + X$ AT 205 GeV/c*

F. C. Winkelmann

Lawrence Berkeley Laboratory
University of California
Berkeley, California 94720

December 5, 1973

ABSTRACT

Characteristics of the reactions $\pi^- p \to p + X$ and $pp \to p + X$ are compared at 205 GeV/c. In the lower multiplicity final states significant differences are observed in the spectrum of M^2, the mass-squared of the produced system X. However, the inclusive reactions show remarkable similarities in the distribution of momentum transfer to the recoil proton and in the dependence on M^2 of the average charged multiplicity of X. Triple-Regge theory with PPP or PRR terms is found to correctly predict the ratio of the inclusive cross sections for $30 \lesssim M^2 \lesssim 120$ GeV^2.

---

*Work supported by the U. S. Atomic Energy Commission.

The inelastic reactions

$$\pi^- p \rightarrow p + X \qquad (1)$$

and

$$pp \rightarrow p + X \qquad (2)$$

have recently been studied at 205 GeV/c in the NAL 30-inch hydrogen bubble chamber [1,2]. These processes were shown to display several striking features, including diffractive-like excitation of the incoming pion or proton into masses up to 5 or 6 GeV. In this Letter, these two reactions are compared using data presented in Refs. [1] and [2], and some important similarities between them are pointed out. The comparison is particularly straightforward since the beam momenta are the same, and the experimental analyses, although performed by different experimental groups, are quite similar.

In the following we emphasize the behavior of the system X as a function of M^2 and t, where M^2 is the mass-squared of X and t is the momentum transfer to the recoil proton. For both reactions the resolution in M^2 is approximately $\pm$ 1.5 GeV^2, and the recoil proton, identified by ionization, is required to have lab momentum $\leq$ 1.4 GeV/c. The dependence on t is such that biases introduced by the cutoff in proton momentum are negligible up to $M^2 \approx 150$ GeV^2.

In Fig. 1 we compare the distributions in M^2 for charged multiplicity 2, 4, 6, 8, and $\geq$ 10 for reactions (1) and (2). We note the following features:

(1) Both reactions show prominent diffractive enhancements in the 2-, 4-, and 6-prong events which extend to about 30 GeV^2. For higher masses, the M^2 distributions are smooth and featureless.

(2) The beam diffractive cross section for both reactions comes predominantly from the 2- and 4-prong events, with a small contribution from the 6-prongs.

(3) A difference between the two reactions can be noted in the relatively large ratio of proton to pion diffraction for $M^2 \lesssim 5$ GeV^2 in the 2-prongs.

This is probably due in part to the fact that the proton can diffractively dissociate into two particles ($p\pi^o$ and $n\pi^+$, for example) whereas the pion is constrained by G-parity to dissociate into at least three pions.

(4) The 4-prong diffractive peaks for reactions (1) and (2) differ significantly in position and shape, due presumably to G-parity effects, as in the 2-prongs, as well as differences in the masses, thresholds, couplings, etc., of the pionic and baryonic "resonances" which contribute to the peaks.

(5) Beam dissociation in the 4-prong exclusive reactions $\pi^- p \to p\pi^+\pi^-\pi^-$ [3] and $pp \to pp\pi^+\pi^-$ [4] is confined almost entirely to $M^2 < 10$ GeV^2 (where these processes each contribute about 60% of the 4-prong events of reactions (1) and (2), respectively). Above 10 GeV^2, therefore, the incoming pion and proton both dissociate predominantly into three charged particles plus neutrals.

(6) The pion and proton diffraction peaks in the 6-prong topology are both substantially broader than the 2- and 4-prong peaks.

The inclusive M^2 distributions for reactions (1) and (2) are compared in Fig. 2a, and Fig. 2b shows the ratio, R, of the inclusive cross sections as a function of M^2:

$$R(M^2) = \frac{d\sigma/dM^2(\pi^- p \to pX)}{d\sigma/dM^2(pp \to pX)} .$$

(It should be noted that, above $M^2 \approx 150$ GeV^2, the M^2 distributions and, therefore, R, are biased as a result of the 1.4 GeV/c cutoff in proton momentum.) Below 10 GeV^2, in the region of the pronounced low-mass peaks in the 2- and 4-prong events, R has an average value of 0.88±0.06. Thus, at 205 GeV/c, pions and protons have nearly equal cross sections for single diffraction dissociation into low-mass states. Above 10 GeV^2, R is substantially smaller, and is quite consistent with being independent of M^2 for $30 \lesssim M^2 \lesssim 120$ GeV^2, with an average value in this region of 0.63±0.04. A similar trend is observed for the individual topologies, where the cross-section ratios between 30 and 120 GeV^2 are consistent with being M^2-independent

(see Fig. 1), with average values of 0.45±0.08, 2-prongs; 0.48±0.05, 4-prongs; 0.56±0.06, 6-prongs; 0.65±0.07, 8-prongs; and 0.95±0.12, ≧ 10-prongs.

An M^2-independent value of R in good agreement with the inclusive data between 30 and 120 GeV^2 is predicted by triple-Regge theory. Mueller-Regge diagrams [5] for reactions (1) and (2) are shown in Fig. 3a and b. Choosing trajectory j to be the Pomeron (P), which is expected to be reasonable for $M^2 \gtrsim 30$ GeV^2, gives the following ratio of differential cross sections [6]:

$$R(s,t,M^2) = \frac{d\sigma/dM^2dt(\pi^- p \to pX)}{d\sigma/dM^2dt(pp \to pX)} = \frac{\sum_i g^2_{ipp}(t)\, g_{P\pi\pi}(0)\, g_{iiP}(t)\left(\frac{s}{M^2}\right)^{2\alpha_i(t)} (M^2)^{\alpha_P(0)}}{\sum_i g^2_{ipp}(t)\, g_{Ppp}(0)\, g_{iiP}(t)\left(\frac{s}{M^2}\right)^{2\alpha_i(t)} (M^2)^{\alpha_P(0)}}$$

$$= \frac{g_{P\pi\pi}(0)}{g_{Ppp}(0)} \quad . \qquad (3)$$

Here, s is the square of the center-of-mass energy, which is taken to be equal for reactions (1) and (2); the g's are couplings, and the α's are trajectory functions. The summation is over the same set of trajectories i for both reactions. We see that R does not depend on which trajectories i are involved and reduces to a constant equal to the ratio of the $P\pi\pi$ and Ppp couplings at $t = 0$. This ratio, in turn, can be obtained from the measured elastic $\pi^- p$ and pp cross sections at 205 GeV/c assuming elastic scattering at this energy proceeds by factorizable Pomeron exchange:

$$R = g_{P\pi\pi}(0)/g_{Ppp}(0) = \left[\frac{\sigma_{e\ell}(\pi^- p)}{\sigma_{e\ell}(pp)}\right]^{1/2} = 0.66\pm0.03 \quad ,$$

using $\sigma_{e\ell}(\pi^- p) = 3.0\pm0.3$ mb [7] and $\sigma_{e\ell}(pp) = 6.8\pm0.2$ mb [2]. The predicted value of R, shown by the dashed horizontal line in Fig. 2b, is in excellent agreement with the measured average ratio of 0.63±0.04 for $30 < M^2 < 120$ GeV^2.

We turn now to a comparison of the t-dependence of reactions (1) and (2).

As shown in Refs. [1] and [2], $d\sigma/dtdM^2$ for both reactions is consistent with a simple exponential dependence of the form Ae^{Bt} for $-t \lesssim 0.5$ GeV^2, with a slope B that depends on M^2. Figure 4 compares fitted values of B as a function of M^2. The slopes for both reactions are quite similar over the entire range of M^2 shown. B is observed to fall rapidly from about 9 GeV^{-2} for $M^2 \lesssim 5$ GeV^2 to a nearly-constant value of about 6 GeV^{-2} between 10 and 100 GeV^2. As with the cross-section ratio R, the region of rapid variation of B is below 10 GeV^2. For higher masses, the agreement in slopes is consistent with the t-independence of the $d\sigma/dtdM^2$ ratio predicted by the triple-Regge model (see Eq. (3)).

Finally, Fig. 5 shows a comparison of the average charged multiplicity, $\langle n_x \rangle$, as a function of M^2 for the system X in reactions (1) and (2). The two processes give remarkably similar values of $\langle n_x \rangle$ over a broad range of mass extending from threshold to 200 GeV^2. Thus, the charged multiplicity of the produced system is strongly mass-dependent but is insensitive to the nature of the incoming beam particle. A similar effect is well known for inelastic processes of the type

$$\text{hadron} + \text{hadron} \rightarrow \text{anything} \quad ,$$

where the average charged multiplicity is approximately universal in the sense that it depends on total energy but only weakly on the initial hadrons. If the system X in reactions (1) and (2) is produced by an interaction between the incoming beam and an exchanged virtual hadron, as in the multiperipheral model [8], then this universality could be applicable and would explain the observed agreement in $\langle n_x \rangle$ for these reactions.

In conclusion, we have shown that, aside from differences in the details of the beam-diffractive "resonance" regions, some very close similarities exist between the reactions $\pi^- p \rightarrow p + X$ and $pp \rightarrow p + X$ at 205 GeV/c.

It is a pleasure to thank G. Goldhaber for helpful discussions.

REFERENCES

1. F. C. Winkelmann, G. S. Abrams, H. H. Bingham, D. M. Chew, B. Y. Daugéras, W. B. Fretter, C. E. Friedberg, G. Goldhaber, W. R. Graves, A. D. Johnson, J. A. Kadyk, L. Stutte, G. H. Trilling, G. P. Yost, D. Bogert, R. Hanft, F. R. Huson, D. Ljung, C. Pascaud, S. Pruss, and W. M. Smart, LBL-2113 (October 1973).
2. S. J. Barish, D. C. Colley, P. F. Schultz, and J. Whitmore, Phys. Rev. Letters 31, 1080 (1973).
3. G. S. Abrams et al., LBL-2112 (August 1973).
4. M. Derrick, B. Musgrave, P. Schreiner, and H. Yuta, ANL/HEP 7332 (1973).
5. For a review of Mueller-Regge analysis see W. R. Frazer et al., Rev. Mod. Phys. 44, 284 (1972).
6. A similar ratio has been derived from triple-Regge theory by J. Dash, RLO-1388-660 (July 1973).
7. D. Bogert et al., Phys. Rev. Letters 31, 1271 (1973).
8. See, for example, C. F. Chan, Phys. Rev. D8, 179 (1973).

FIGURE CAPTIONS

Fig. 1. Distributions in missing-mass squared, M^2, for $\pi^- p \to p + X$ (dashed histograms) and $pp \to p + X$ (solid histograms) for inelastic 2-, 4-, 6-, 8- and $\geq$ 10-prong events. Representative statistical error bars are shown.

Fig. 2. (a) Inclusive M^2 distribution, $d\sigma/dM^2$, for inelastic $\pi^- p \to p + X$ (dashed histogram) and $pp \to p + X$ (solid histogram). (b) Ratio of the distributions in (a), $[d\sigma/dM^2(\pi^- p \to p + X)]/[d\sigma/dM^2(pp \to p + X)]$. The triple-Regge model prediction for this ratio is M^2-independent with a value of $(\sigma^{e\ell}_{\pi^- p}/\sigma^{e\ell}_{pp})^{1/2} = 0.66 \pm 0.03$ (dashed horizontal line), in good agreement with the data for $30 \lesssim M^2 \lesssim 120$ GeV^2.

Fig. 3. Mueller-Regge diagrams for (a) $\pi^- p \to p + X$ and (b) $pp \to p + X$. Trajectory j is taken as the Pomeron (P) and the trajectories i are the same for both reactions. For given trajectory i (Pomeron or Regge) and center-of-mass energy $\sqrt{s}$, (a) and (b) differ only in the couplings $g_{P\pi\pi}(0)$ and $g_{Ppp}(0)$ at the lower vertex.

Fig. 4. Comparison of the exponential slope, B, of the differential cross section $d\sigma/dtdM^2$ as a function of M^2 for inelastic $\pi^- p \to p + X$ (open circles) and $pp \to p + X$ (solid circles).

Fig. 5. Comparison of the average charged multiplicity, $\langle n_x \rangle$, for the system X as a function of the mass-squared, M^2, of X for the inelastic reactions $\pi^- p \to p + X$ (open circles) and $pp \to p + X$ (solid circles).

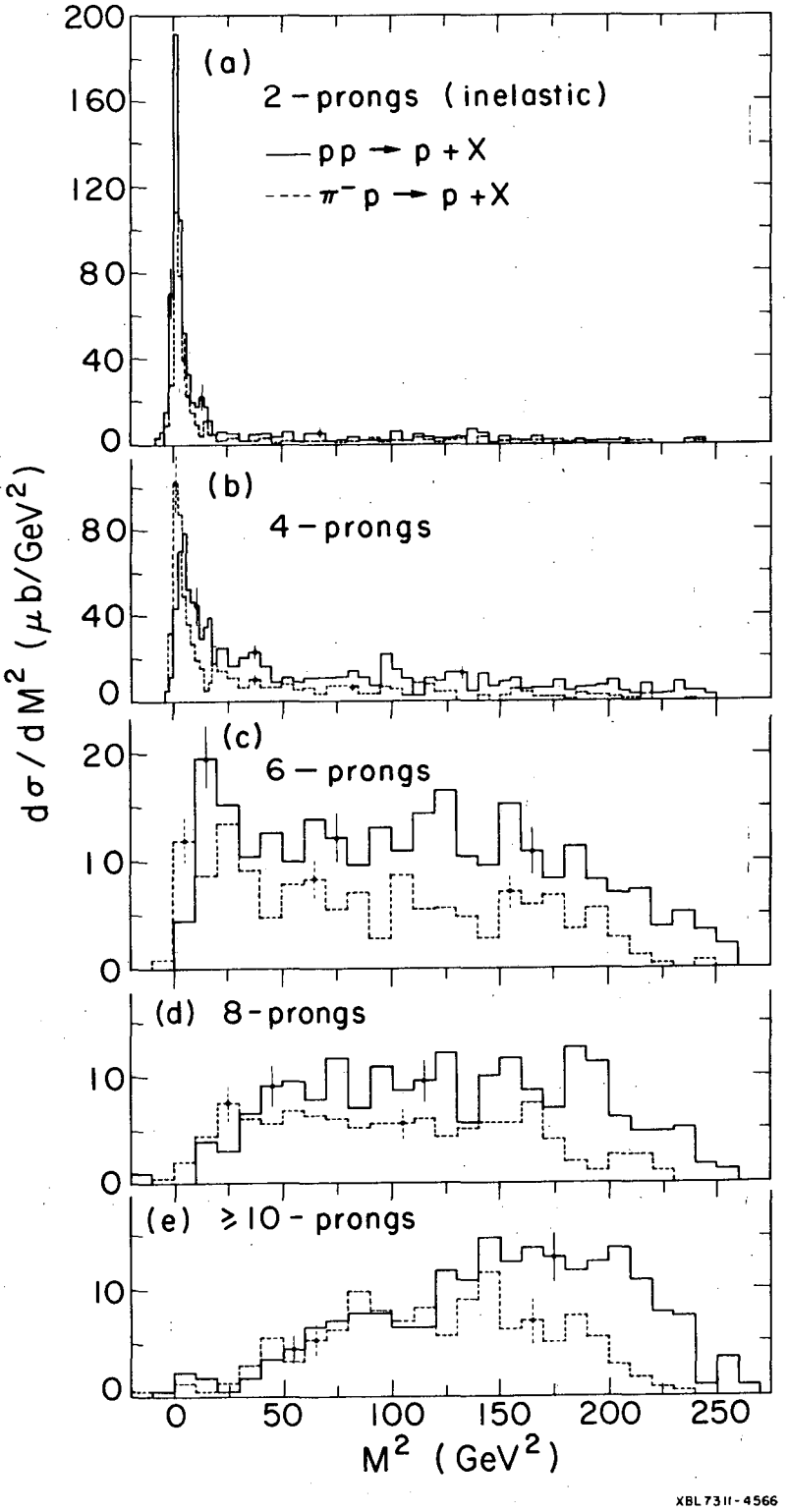
(a)
2-prongs (inelastic)
pp → p + X
π⁻p → p + X
(b)
4-prongs
(c)
6-prongs
(d) 8-prongs
(e) ≥ 10-prongs
dσ/dM² (μb/GeV²)
M² (GeV²)
XBL7311-4566

Fig. 1

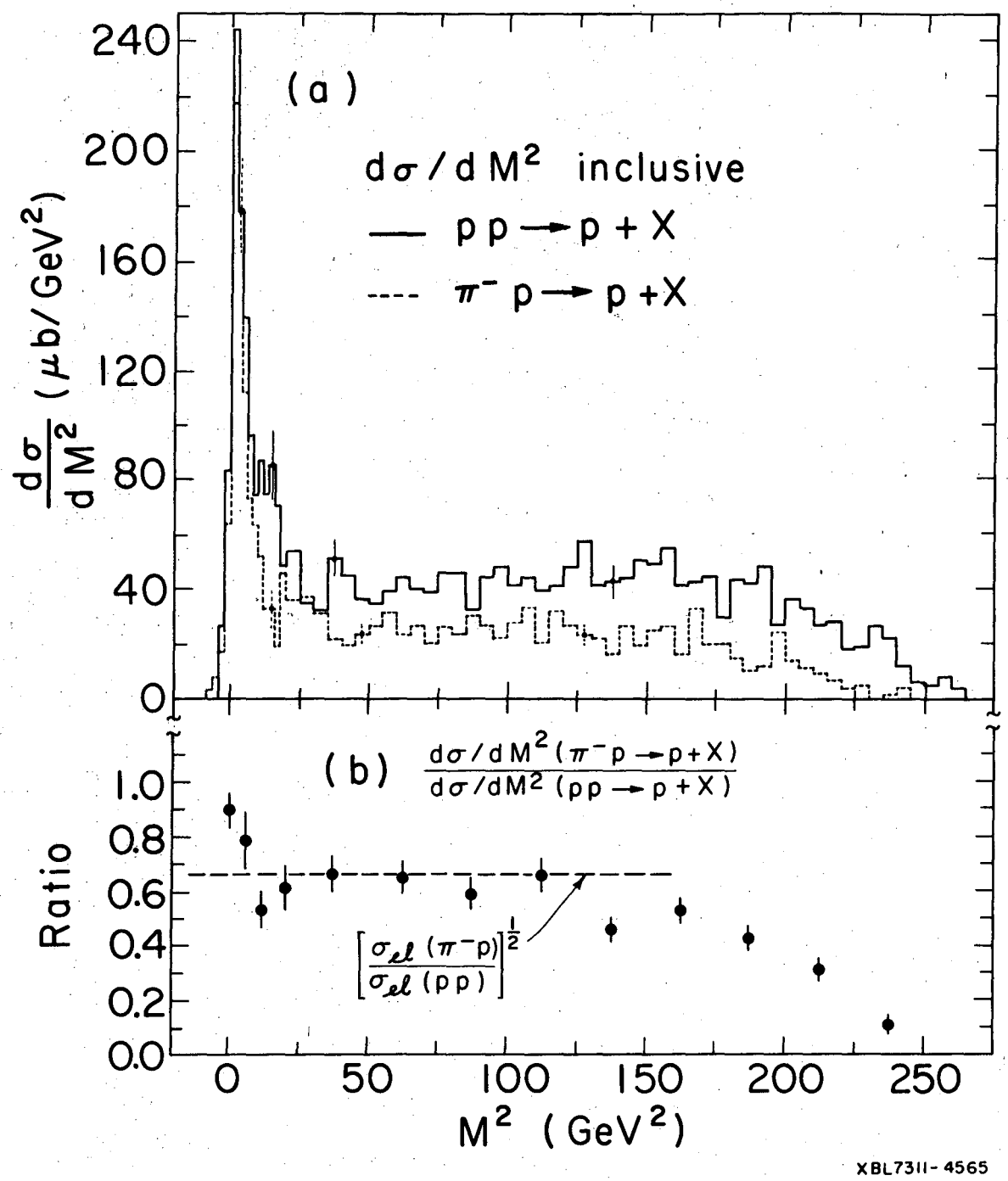
(a)
dσ/dM² inclusive
pp → p + X
π⁻p → p + X
dσ/dM² (μb/GeV²)
240
200
160
120
80
40
0
(b)
dσ/dM²(π⁻p → p+X) / dσ/dM²(pp → p+X)
Ratio
1.0
0.8
0.6
0.4
0.2
0.0
[σel(π⁻p)/σel(pp)]^½
0
50
100
150
200
250
M² (GeV²)
XBL7311-4565

Fig. 2

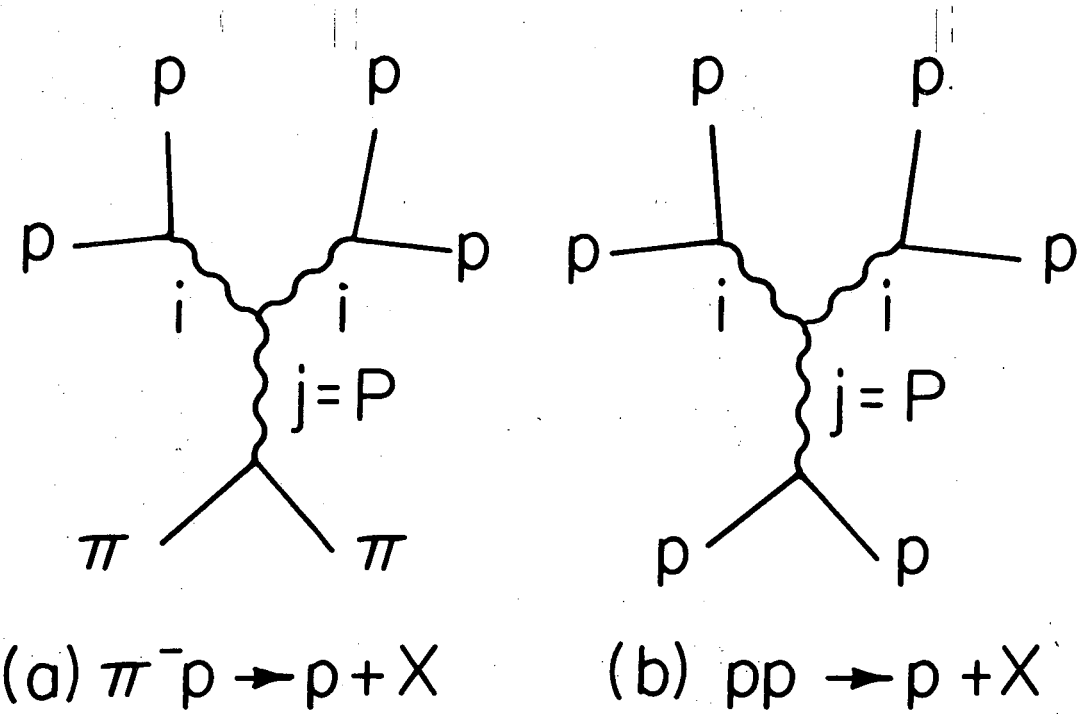

Fig. 3

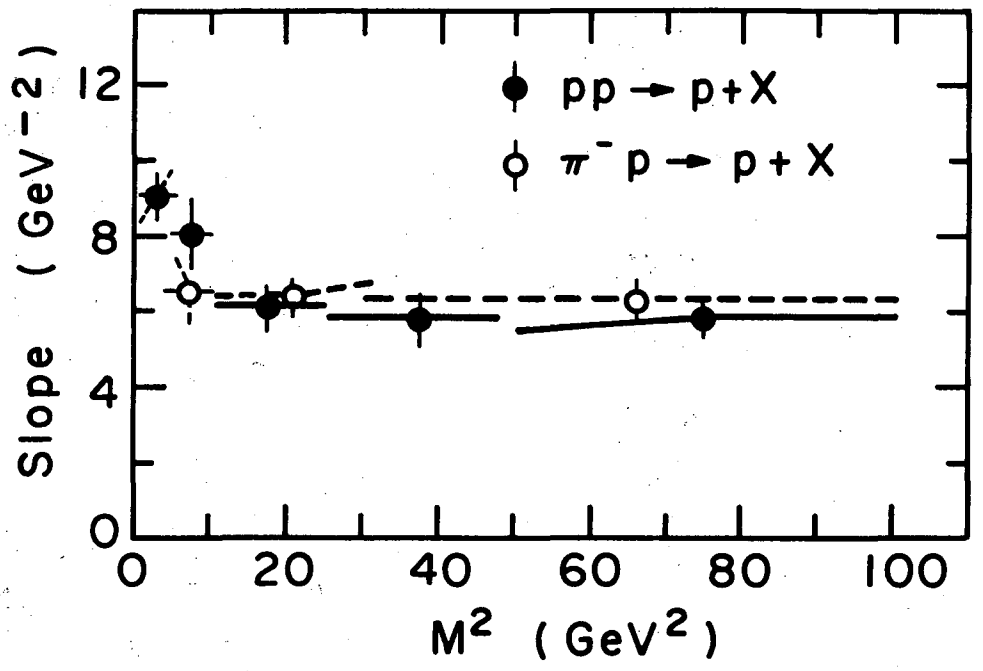
Slope (GeV⁻²)
12
8
4
0
0
20
40
60
80
100
M² (GeV²)
pp → p+X
π⁻p → p+X
XBL7311-4569

Fig. 4

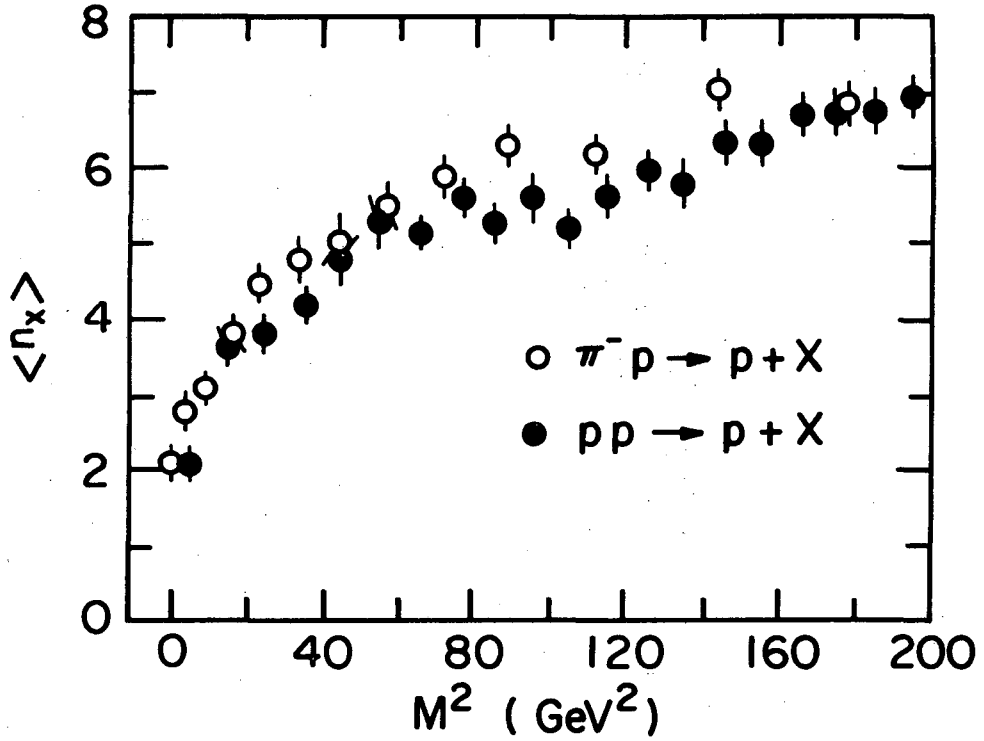
8
6
4
2
0
$\langle n_x \rangle$
0
40
80
120
160
200
M^2 (GeV^2)
$\pi^- p \rightarrow p + X$
$pp \rightarrow p + X$
XBL7311-4568

Fig. 5

TECHNICAL INFORMATION DIVISION
LAWRENCE BERKELEY LABORATORY
UNIVERSITY OF CALIFORNIA
BERKELEY, CALIFORNIA 94720